Impact of thin film metrology on the lithographic performance of 193nm bottom antireflective coatings

Chris A. Mack[a], Dale Harrison[b], Cristian Rivas[b], and Phillip Walsh[b]
[a]Lithoguru.com, Austin, TX
[b]MetroSol, 2101 Donley Drive, Suite 101, Austin, TX 78758 USA

ABSTRACT

The performance needs of a bottom antireflection coating (BARC) used in advanced optical lithography are extremely demanding, with reflectivities as low as 0.1% and even lower often required. BARC thickness and complex refractive index values ($\boldsymbol{n} = n + i\kappa$) must be highly optimized, requiring accurate knowledge of the BARC, resist and substrate optical properties. In this paper, we have performed a theoretical analysis of the BARC optimization process with respect to the propagation of BARC n and κ measurement errors. For several realistic cases, specifications on the measurement accuracy of these optical parameters will be derived and the lithographic consequences of BARC metrology errors will be explored. Approaches to improving the measurement of BARC thickness and refractive index will be suggested.

Keywords: Bottom antireflection coating, BARC, refractive index measurement, vacuum ultra-violet reflectometry, PROLITH

1. Introduction

At 65nm device generations and below, requirements for bottom antireflection coating (BARC) performance are extremely stringent. Reflectivities less than 0.1% are often required. BARC thickness and complex refractive index values must be highly optimized for the specific resist, film stack, and even for the feature size and lithographic imaging parameters being used. Implicit in the optimization procedure is the assumption that the optical properties of the BARC have been measured to sufficient accuracy so that the uncertainty in the measurement of these BARC properties will not have a significant impact on the lithographic performance of the resulting optimized BARC.

In this paper, we will perform a theoretical analysis of the BARC optimization process with respect to the propagation of BARC n and κ (the real and imaginary parts of the refractive index) measurement errors. For several realistic cases, specifications on the measurement accuracy of these optical parameters will be derived and the lithographic consequences of BARC metrology errors will be explored. Next, the impact of measurement noise on the uncertainty of n and κ measurements will be studied for the case of spectral reflectance-based measurements. In particular, the influence of measurement wavelength range will be shown to have a significant impact on the propagation of measurement noise to uncertainty in BARC n and κ values. Finally, the lithographic impact of BARC measurement choices will be shown as a propagation of measurement uncertainty to an increase in final substrate reflectivity. The goal of this paper is to present a comprehensive method for evaluating the impact of measurement noise on the lithographic performance of BARC materials.

2. Theory of BARC Optimization

The goals of film stack optimization are to minimize standing waves in the resist, and to reduce the sensitivity of the process to film stack variations (including resist, but other layers as well). By far the most common way to accomplish all of these goals is by using an optimized BARC. When optimizing a litho process for reflectivity, there are three basic tasks: 1) optimize the BARC, 2) optimize the resist thickness (from a swing curve perspective), and 3) understand the sensitivity to BARC, resist, and film stack variations. For the first task, there are two classes of BARC problems:

- BARC on an absorbing substrate (such as metal) – the goal is to reduce the reflectivity (the thickness of the metal or what's underneath doesn't matter)
- BARC on a transparent substrate (such as silicon dioxide) – reduce the sensitivity to oxide thickness variations (while also keeping reflectivity low)

There is an unfortunate problem in that the substrate reflectivity experienced by the photoresist cannot be measured. Measuring the reflectivity of the substrate when not coated by photoresist is not useful to this task, and once coated the reflectivity becomes hidden from measurement. Thus, the approach that must be used is to calculate the reflectivity from measured fundamental parameters, namely the thickness and complex refractive index of each layer in the film stack.

There are three BARC parameters available for optimization: the thickness of the BARC, and the real and imaginary parts of its refractive index. The treatment below follows that given in Reference 1.

BARC on an Absorbing Substrate

The electric field reflection coefficient (the ratio of reflected to incident electric fields) at the interface between two materials is a function of the complex indices of refraction for the two layers. For normal incidence, the reflection coefficient of light traveling through layer *i* and striking layer *j* is given by

$$\rho_{ij} = \frac{\boldsymbol{n}_i - \boldsymbol{n}_j}{\boldsymbol{n}_i + \boldsymbol{n}_j} \tag{1}$$

where $\boldsymbol{n}$ is the complex refractive index ($\boldsymbol{n} = n + i\kappa$). For the case of a bottom antireflection coefficient (BARC), assume the BARC (layer 2) is sandwiched between a resist (layer 1) and a very thick substrate (layer 3). The total reflectivity looking down on layer 2 includes reflections from both the top and bottom of the BARC film. The resulting reflectivity, taking into account all possible reflections, is

$$R_{total} = \left|\rho_{total}\right|^2 = \left|\frac{\rho_{12} + \rho_{23}\tau_D^2}{1 + \rho_{12}\rho_{23}\tau_D^2}\right|^2 \tag{2}$$

where the internal transmittance, τ_D, is the change in the electric field as it travels from the top to the bottom of the BARC, given by

$$\tau_D = e^{i2\pi \boldsymbol{n}_2 D/\lambda} \tag{3}$$

for a BARC of thickness D.

If the role of layer 2 is to serve as an antireflection coating between materials 1 and 3, one obvious requirement might be to minimize the total reflectivity given by equation (2). If the light reflecting off the top of layer 2 (ρ_{12}) can cancel out the light that travels down through layer 2, reflects off layer 3, and then travels back up through layer 2 ($\rho_{23}\tau^2_D$), then the reflectivity can become exactly zero. In other words,

$$R_{total} = 0 \quad \text{when} \quad \rho_{12} + \rho_{23}\tau_D^2 = 0 \quad \text{or} \quad \rho_{21} = \rho_{23}\tau_D^2 \tag{4}$$

When designing a BARC material, there are only three variables that can be adjusted: the real and imaginary parts of the refractive index of the BARC, and its thickness. One classic solution to equation (4) works perfectly when the materials 1 and 3 are non-absorbing: let τ^2_D = -1 and $\rho_{12} = \rho_{23}$. This is equivalent to saying that the BARC thickness is a 'quarter wave' ($D = \lambda/4n_2$), and the non-absorbing BARC has a refractive index of $n_2 = \sqrt{n_1 n_3}$. While this BARC solution is ideal for applications like antireflective coatings on lens surfaces, it is not particularly useful for common lithography substrates, which are invariably absorbing.

Will a solution to equation (4) always exist, even when the resist and substrate have complex refractive indices? Since all the terms in equation (4) are complex, zero reflectivity occurs when both the real part and the imaginary part of equation (4) are true. This requirement can be met by adjusting only two of the three BARC parameters (n, κ, and D). In other words, there is not just one solution but a family of solutions to the optimum BARC problem. Expressing each reflection coefficient in terms of magnitude and phase,

$$\rho_{ij} = \left|\rho_{ij}\right| e^{i\theta_{ij}} \tag{5}$$

equation (4) can be expressed as two equalities:

$$D = \frac{\lambda}{4\pi\kappa_2} \ln\left|\frac{\rho_{23}}{\rho_{21}}\right| = \frac{\lambda}{4\pi n_2}\left(\theta_{21} - \theta_{23}\right) \tag{6}$$

Unfortunately, the seemingly simple forms of equations (4) and (6) are deceptive: solving for the unknown complex refractive index of the BARC is exceedingly messy. As a consequence, numerical solutions to equation (4) or (6) are almost always used. Note that a second-minimum BARC can be optimized using equation (6) by adding 2π to the angle difference on the right hand side of the equation.

Consider a common case of a BARC for 193nm exposure of resist on silicon. The ideal BARC is the family of solutions as shown in Figure 1, which gives the ideal BARC n and κ values as a function of BARC thickness. Each solution produces exactly zero reflectivity for normally incident monochromatic light. Within this family of solutions, available materials and the acceptable range of BARC thicknesses (usually constrained by coating and etch requirements) will dictate the final solution chosen.

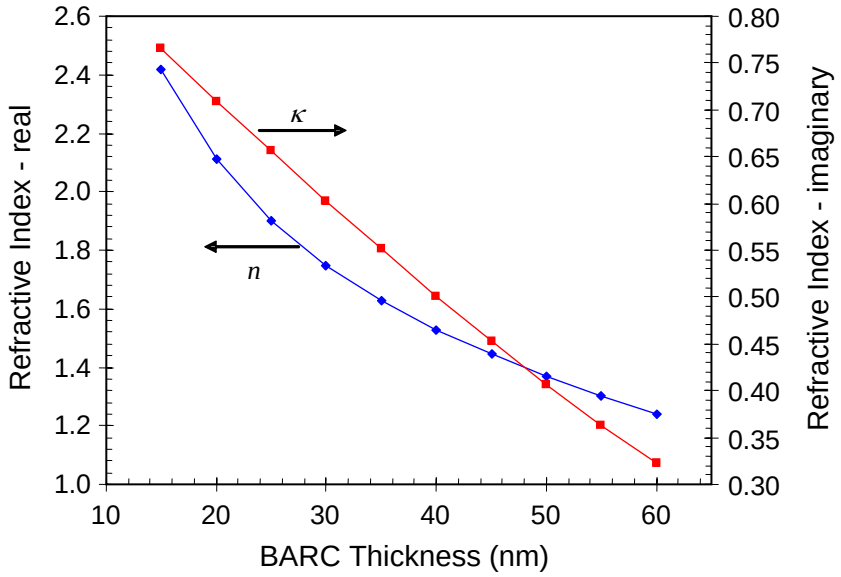

(a)

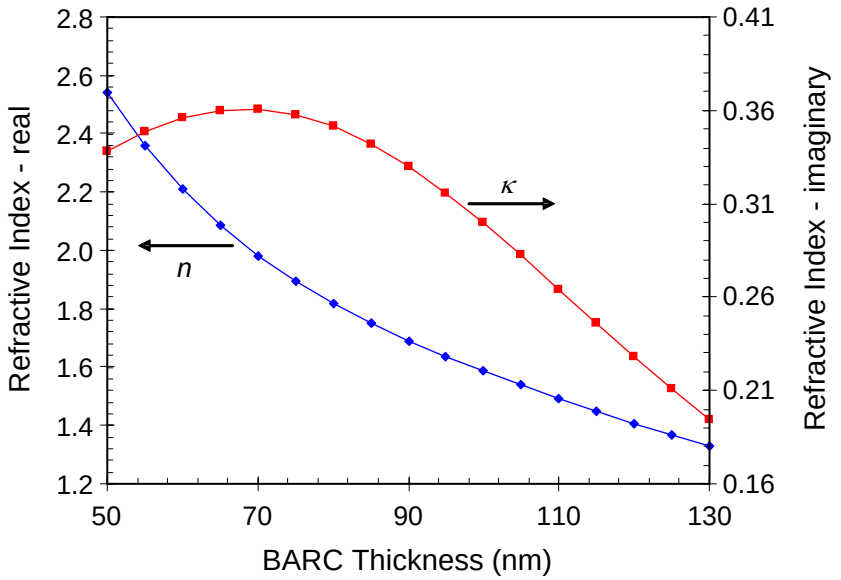

(b)

Figure 1 Optimum BARC refractive index (real and imaginary parts, n and κ) as a function of BARC thickness for normal incidence illumination (resist index = 1.7 + i0.01536 and silicon substrate index = 0.8831 + i2.778) at 193nm. a) First minimum BARCs, and b) second minimum BARCs.

Another criterion for choosing the optimum BARC is the sensitivity to BARC thickness variations. Often, BARC layers are coated over topography and are partially planarizing. This means that BARC thickness variations across the device are inevitable. Is one BARC solution from the family of solutions given in Figure 1 better from a BARC thickness sensitivity perspective? Consider only small errors in

BARC thickness about the optimum value, so that $D = D_{opt} + \Delta$ where D_{opt} is the optimum thickness given by equation (6). Since equation (4) is true at the optimum thickness,

$$\rho_{12} + \rho_{23}\tau_D^2 = \rho_{12} + \rho_{23}\tau_{D_{opt}}^2 e^{i4\pi \boldsymbol{n}_2 \Delta/\lambda} = \rho_{12}\left(1 - e^{i4\pi \boldsymbol{n}_2 \Delta/\lambda}\right) \tag{7}$$

Using a similar operation on the denominator of the reflectivity expression (2) gives

$$R = \left| \frac{\rho_{12}\left(1 - e^{i4\pi \boldsymbol{n}_2 \Delta/\lambda}\right)}{1 - \rho_{12}^2 e^{i4\pi \boldsymbol{n}_2 \Delta/\lambda}} \right|^2 \tag{8}$$

Assuming Δ is small, keeping only the first two terms of a Taylor's expansion of the exponential in the numerator gives

$$R \approx \Delta^2 \left(\frac{\pi n_1}{\lambda}\right)^2 \left| 1 - \left(\frac{\boldsymbol{n}_2}{\boldsymbol{n}_1}\right)^2 \right|^2 \tag{9}$$

As can be seen, the reflectivity increases approximately quadratically about the optimum BARC thickness. Different BARC solutions will have different sensitivities, depending on how close the ratio $\boldsymbol{n}_2/\boldsymbol{n}_1$ is to one. For the first minimum BARC example in Figure 1, the ~50nm BARC thickness solution has the minimum sensitivity to BARC thickness errors.

Similarly, variations in refractive index of a BARC can cause the reflectivity of an otherwise optimal BARC solution to increase. For the case of the optimal normal-incidence BARC, the reflectivity for a given change is BARC index $\Delta\boldsymbol{n}$ (which can be an error in real and/or imaginary parts) will be approximately

$$R \approx \left|\Delta \boldsymbol{n}\right|^2 \left| \frac{\rho_{12}}{1 - {\rho_{12}}^2} \right|^2 \left| \frac{1 + \rho_{12}}{\boldsymbol{n}_1 - \boldsymbol{n}_2} + \frac{1 - \rho_{23}}{\boldsymbol{n}_2 - \boldsymbol{n}_3} + i4\pi D/\lambda \right|^2 \tag{10}$$

Note that $\left|\Delta \boldsymbol{n}\right|^2$ is the sum of the squares of the errors in the real and imaginary parts of the index. The sensitivity to BARC errors, either in thickness or in refractive index, are shown in Figures 2 and 3 for the case of the BARC solutions of Figure 1. Note that for this case, practical first minimum BARC solutions have thicknesses in the 20 – 50 nm range. Thus, for this case, thicker BARCs are less sensitive to thickness errors but more sensitive to refractive index errors. Assuming that a reflectivity of 0.1% can be tolerated, a 20 nm optimal BARC can tolerate 1 nm of thickness error, or a 0.053 change in refractive index. A 40 nm optimal BARC can tolerate 2 nm of thickness error, or a 0.04 change in refractive index. Roughly, if the BARC thickness has no error, the real part of the refractive index of these BARCs must be controlled to 2.5% assuming no error in the imaginary part, or the imaginary parts must be controlled to 8% for no error in the real part. Likewise, if the refractive index has no error, the BARC thickness must be controlled to roughly 5% for the given 0.1% reflectivity tolerance.

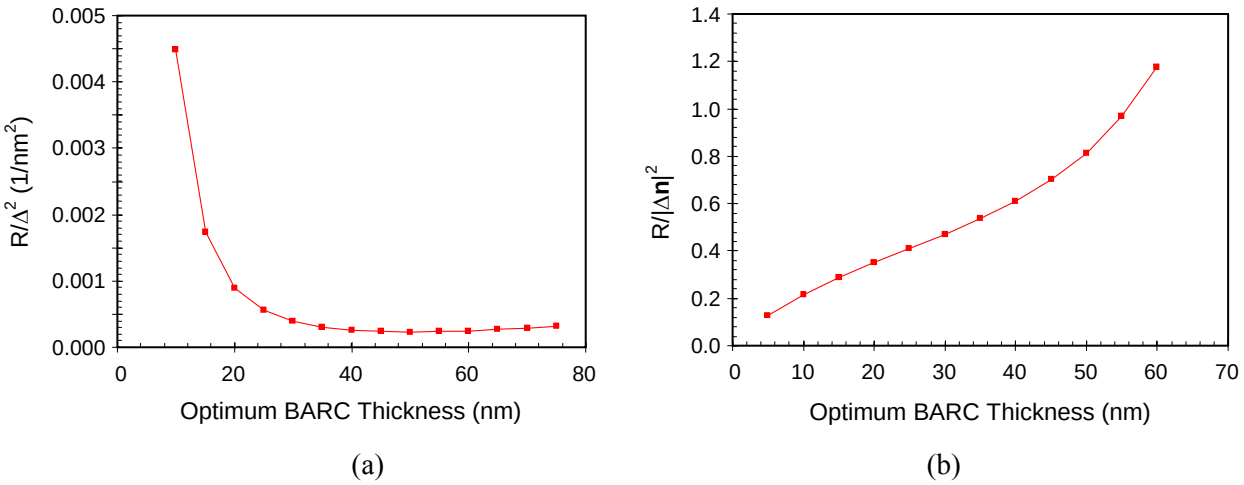

(a) (b)

Figure 2 Sensitivity of substrate reflectivity for the optimum BARCs of Figure 1a as a function of a) BARC thickness errors, or b) BARC refractive index errors.

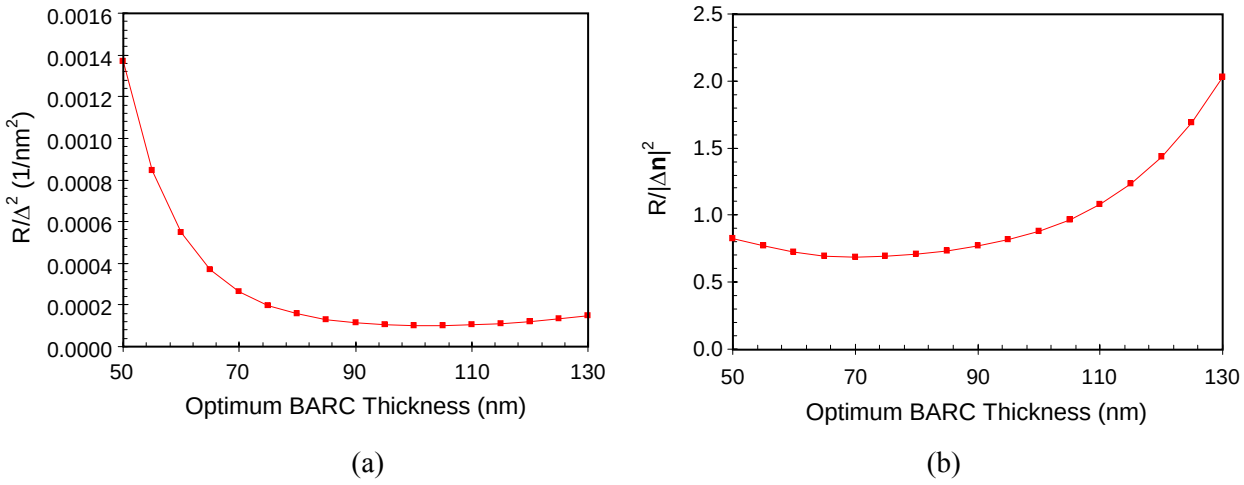

(a) (b)

Figure 3 Sensitivity of substrate reflectivity for the optimum second minimum BARCs of Figure 1b as a function of a) BARC thickness errors, or b) BARC refractive index errors.

BARC on a Transparent Substrate

The second type of BARC optimization problem involves the use of a BARC on a transparent substrate, such as an oxide film. For such a case, the overall substrate reflectivity will be a function of the oxide thickness and one of the goals of the BARC design is to reduce the sensitivity to underlying film thickness variations. As can be seen from Figure 4, using the BARC at a first minimum results in a very large sensitivity to underlying oxide thickness variations. In fact, the thickest BARC films provide the most robust behavior when a wide range of oxide thicknesses are expected. Thus, the preferred design approach for this case is to determine the maximum allowed BARC thickness from an integration perspective, then optimize the n and κ values of the BARC to minimize the maximum reflectivity over the range of expected oxide thicknesses.

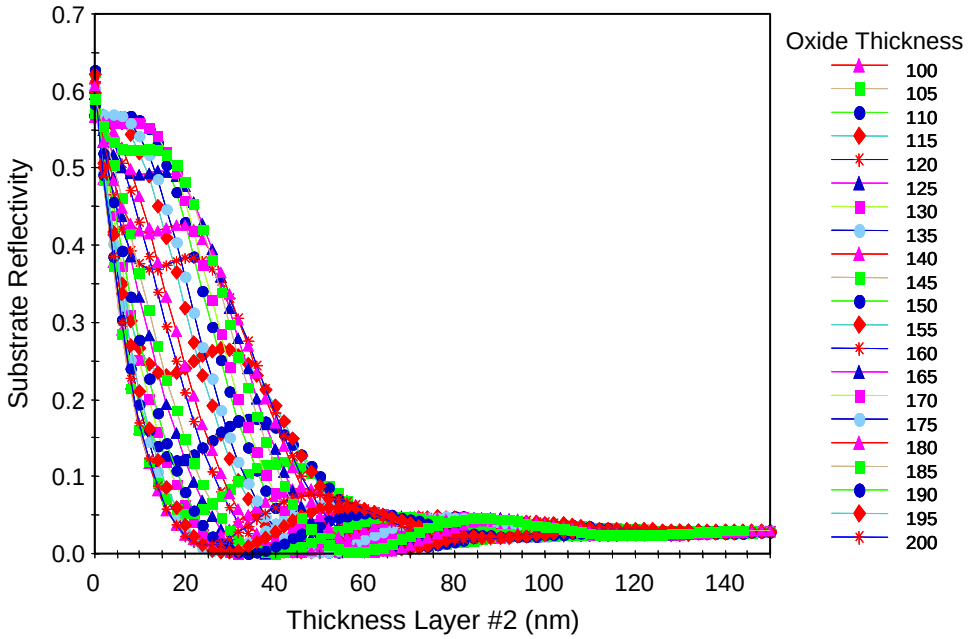

Figure 4 Substrate reflectivity versus BARC thickness over a range of underlying oxide thicknesses (oxide on top of a silicon substrate).

A 'thick' BARC solution can be thought of as a BARC that completely absorbs all of the light that may reflect off the substrate and is thus insensitive to changes in the substrate stack. For this case, the product of BARC thickness and the imaginary part of its refractive index (κ_2) must be sufficiently high. Maximum BARC thickness is usually determined by process considerations, thus fixing the minimum κ_2. Assuming the imaginary part of the resist refractive index is sufficiently small, the resulting reflectivity is

$$R_{total} = \left|\rho_{12}\right|^2 = \left|\frac{n_1 - n_2 - i\kappa_2}{n_1 + n_2 + i\kappa_2}\right|^2 = \frac{(n_1 - n_2)^2 + {\kappa_2}^2}{(n_1 + n_2)^2 + {\kappa_2}^2} \tag{11}$$

The optimum real part of the BARC refractive index to minimize reflectivity will then be

$$n_2 = \sqrt{{n_1}^2 + {\kappa_2}^2} \tag{12}$$

The resulting reflectivity is

$$R = \frac{n_2 - n_1}{n_2 + n_1} \approx \frac{{\kappa_2}^2}{4{n_1}^2 + {\kappa_2}^2} \tag{13}$$

Obviously, the thick BARC solution is insensitive to BARC thickness variations by design. The sensitivity to errors in BARC refractive index can be obtained from equation (11). For a small change in the real part of the BARC refractive index,

$$\frac{\Delta R}{R} \approx \Delta {n_2}^2 \frac{n_1}{n_2\left({n_2}^2 - {n_1}^2\right)} = \Delta {n_2}^2 \frac{n_1}{n_2 {\kappa_2}^2} \tag{13}$$

For a small change in the imaginary part of the BARC refractive index,

$$\frac{\Delta R}{R} \approx \frac{\Delta \kappa_2}{\kappa_2}\left(\frac{2n_1}{n_2}\right) \tag{14}$$

BARC Performance

How critical is BARC optimization? How low must the substrate reflectivity be before acceptable CD control can be expected? There is no single answer to these questions, since they are process and feature dependent. But consider the example shown in Figure 5. Here, 100 nm lines on a 280 nm pitch are simulated (using PROLITH v9.3) with a stepper using annular illumination, with a center sigma given by σNA = 0.54. As can be seen, a substrate reflectivity of less than 0.1% still leads to a noticeable swing behavior.

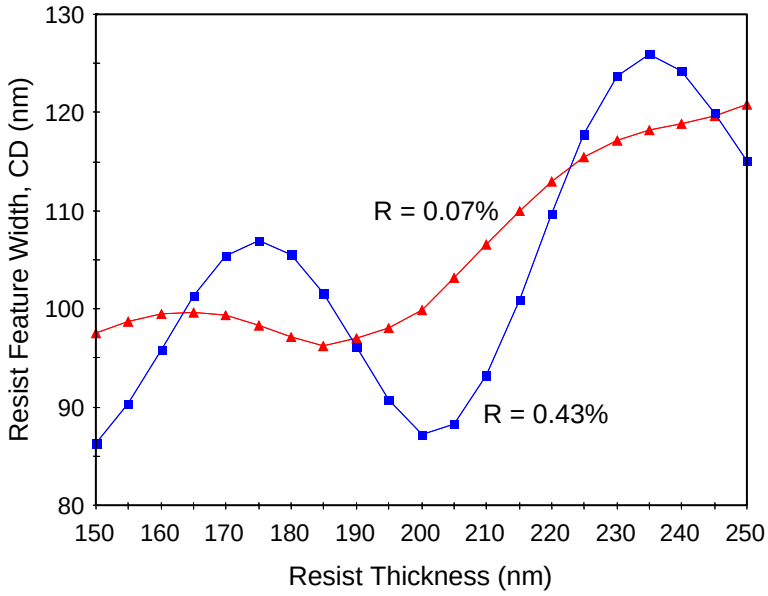

Figure 5 CD swing curves (100nm lines with a 280nm pitch are printed with a stepper using annular illumination, with a center sigma given by σNA = 0.54) for two different BARCs with different levels of optimization, as given by the resulting substrate reflectivity R. (Simulations using PROLITH v9.3.)

A common approach to characterizing the impact of substrate reflectance (that is, the impact of a non-ideal BARC) is to relate reflectivity in the presence of film thickness variations to effective dose errors. Consider a resist thickness $D = D_{min} \pm \Delta$ where D_{min} is the thickness at the swing curve minimum and Δ is

small compared to the swing period. Assuming a reasonably good BARC, the effective dose error due to the resist thickness variation is

$$\frac{\Delta E}{E} \approx \alpha\Delta + 4\left|\rho_{air-resist}\rho_{resist-substrate}\right|e^{-\alpha D}\left(2\pi n_{resist}\Delta/\lambda\right)^2 \tag{15}$$

The dose error comes from a bulk absorption term ($\alpha\Delta$) plus a fraction of the swing amplitude. Consider the standard 193 nm resist on BARC on silicon case described above, with $\alpha = 1.2\ \mu m^{-1}$, $D = 200$nm, $n_{resist} = 1.7$, and $|\rho_{air\text{-}resist}| = 0.26$. For Δ in nanometers,

$$\frac{\Delta E}{E} \approx 0.0012\Delta + 0.0025\left|\rho_{resist-substrate}\right|\Delta^2 \tag{16}$$

For an 8.3 nm increase in resist thickness, the bulk effect causes about a 1% effective dose error. The swing effect will cause another 1% effective dose error for that 8.3 nm resist thickness error if the substrate reflectivity is 0.33%. The maximum allowed substrate reflectivity is a function of the range of resist thickness that must be tolerated and the amount of effective dose error one is willing to accept. Specifications of substrate reflectivity near 0.1% are not uncommon.

3. Simulating Errors in Thin Film Metrology

The thickness and optical properties of photoresist and BARC films are routinely characterized using reflectometry and/or ellipsometry. In practice, many varieties of both techniques exist. Regardless of the specific method employed, the underlying approach typically involves recording the optical response through wavelength from a sample and then analyzing this data in order to obtain values for the thickness and optical properties of the film of interest. The calculated response is usually described using the Fresnel equations in combination with one or more models to describe the optical properties of the material comprising the sample. Once the resist and BARC thicknesses and optical properties are determined, the methods of the preceding section can be used to compute substrate reflectivity.

For reflectance measurements, the discrepancy between the measured and calculated data sets is characterized by the weighted merit function

$$\chi^2 = \frac{1}{N-M}\sum_{i=1}^{N}\frac{1}{\sigma_i^2}\left[y_i - y\left(x_i, \mathbf{a}\right)\right]^2 , \tag{17}$$

which is minimized through use of an iterative optimization or 'fitting' procedure such as the Levenberg-Marquardt method [2]. In equation (17), the y_i are the measured data (i.e., reflectance), the x_i are the independent variable (the wavelength, λ, corresponding to data point y_i), σ_i is an estimate of the uncertainty in y_i, **a** is the set of model parameters, N is the number of data points, and M is the number of parameters in the set **a** that are to be optimized. The best fit parameters are defined as those that give the smallest value for χ^2.

Assuming the substrate refractive index and thickness can be regarded as known, a typical single film on substrate measurement requires the determination of $2N+1$ unknowns (film thickness plus N pairs of n and κ). This is generally not possible with only N measured data points. Dispersion models that parameterize the behavior of n and κ with respect to wavelength are normally used to reduce the total

number of optimization parameters. The measured parameter set **a** then consists of the film thickness and a usually small set of dispersion parameters. The optimized dispersion parameters are used to compute the n and κ values at the desired wavelengths at the end of the fitting procedure.

An example of a dispersion model is the Tauc-Lorentz model [3]. The Tauc-Lorentz model is based on a combination of the Tauc joint density of states and the Lorentz oscillator. It has advantages over other available dispersion models in that it is Kramers-Kronig and time-reversal symmetry consistent, correctly describes the behavior of κ in the high frequency limit, and is capable of accurately characterizing the dispersion of a wide range of materials [3]. For a simple 1-term Tauc-Lorentz film, such as the 1-term resist example below, the parameter set **a** consists of the resist thickness and the Tauc-Lorentz dispersion parameters E_g, ε_1, A, E_0, and C, for a total of 6 parameters to be determined from each reflectance measurement. The complex index of refraction $\boldsymbol{n} = \boldsymbol{n}(E_g, \varepsilon_1, A, E_0, C, \lambda)$ is calculated from the Tauc-Lorentz model at the end of the fitting procedure. Films having a more complicated dispersion structure, such as the BARC example below, are characterized using multiple Tauc-Lorentz terms, each term representing a peak in the material's absorption spectrum. The total parameter set then consists of the film thickness, the high frequency constant term ε_1, and four additional parameters E_g, A, E_0, and C for each dispersion peak.

The best achievable χ^2 value is generally limited by the applicability of the model, that is, the extent to which the dispersion model actually describes the optical properties of the material. Still, a good merit value is not in itself sufficient to ensure that accurate results have been obtained. In practice, uncertainties in the derived results may also arise as a result of ambiguity or correlations between parameters in the model, meaning that different combinations of dispersion parameters lead to indistinguishable reflectance spectra. These ambiguities in dispersion parameters often lead to ambiguities in the refractive index values that are calculated from them. In addition, lack of sensitivity of the modeled data to parameter changes can lead to uncertainties when determining parameter values.

Generally speaking, inter-parameter correlation may be reduced by providing greater constraint to the fitting process. In reflectometry, greater constraint may be achieved by a variety of means, including adding data measured at different incident angle and polarization conditions and/or multi-sample analysis. In this paper, another means of providing greater constraint is explored, namely the extension of conventional 190-800nm reflectometry – ultra-violet to visible (UV-Vis) wavelengths – into the 120-190nm vacuum ultra-violet (VUV) region. The optical properties of many materials exhibit richer structure (i.e., peaks and valleys) in the VUV region than at UV and visible wavelengths. This can aid both in enhancing sensitivity of reflectance data to changes in film parameters, as well as in reducing inter-parameter correlations, yielding more reliable n and κ measurements, even when n and κ data are needed only for non-VUV wavelengths. It will be demonstrated that there is considerable benefit associated with the extension of reflectometry data sets into the VUV when using such data in material characterization applications, particularly as they relate to the accurate determination of n and κ values at the 193 nm wavelength.

To explore the effects of extending conventional reflectometry into the VUV, several simulations of 193 nm resist and BARC materials were considered. The optical properties of the resist and BARC, based on actual representative material measurements and shown in Figure 6, were assumed to be perfectly described using a one-term and three-term Tauc-Lorentz model, respectively. The reflectance of a 900Å single layer of each material on a crystalline silicon substrate was calculated from 120–1000 nm wavelength range using the assumed parameter values. These reflectance spectra were then used as the basis for creating a series of similar data files with noise added according to a Gaussian distribution with standard deviations of 0.1% and 0.2%. In this sense, the original noiseless data is considered to be the 'true' reflectance of the sample, which can never be realized in an optical measurement, while the data with added noise represents

realized, albeit simulated, representations of the true reflectance. It is important to point out that the noise model assumed for this initial study is consistent with assuming that errors in the raw data are due to random uncorrelated processes, and represents 'best-case' performance for a given noise level since systematic errors and/or model shortcomings are not represented here.

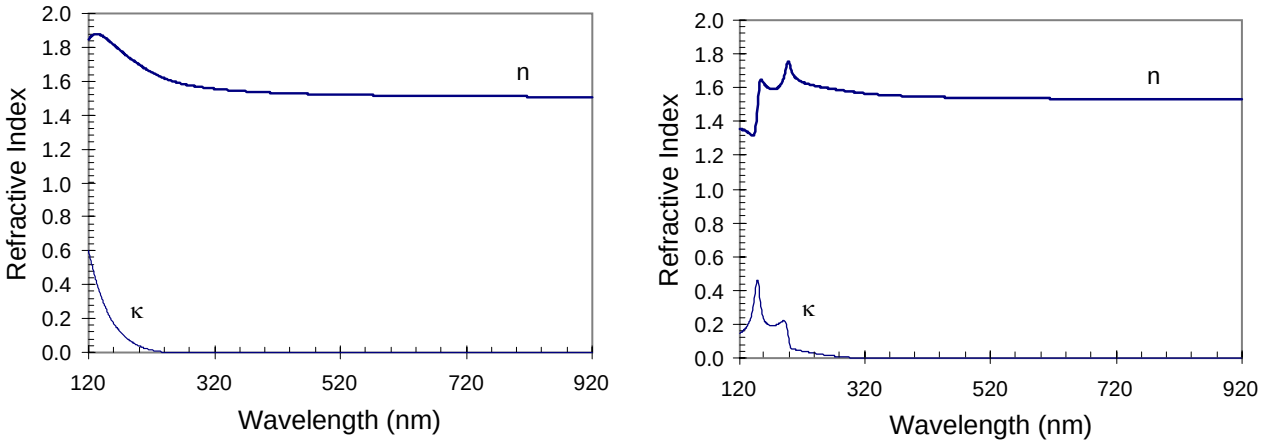

Figure 6 Optical properties used in simulations of a) 1-term photoresist, and b) 3-term BARC materials.

The simulated reflectance data files were analyzed using the Levenberg-Marquardt algorithm in an attempt to re-obtain the starting parameters. To seed the optimization routine, the thickness and Tauc-Lorentz starting parameters were offset by 1% from their nominal values. The final fit parameters were then fed back into the Tauc-Lorentz model and used to calculate the determined values for n and κ at 193 nm. The results of 100 such measurements for each noise condition were used to compute standard 3-σ confidence limits for thickness and 193 nm optical properties.

The results from analysis of the 1-term photoresist reflectance files are summarized in Table 1 and Figure 7 below. The data corresponding to conditions 1 – 3 in Figure 7 correspond to fits performed on simulated data files with a noise level of $1\sigma = 0.2\%$. The first two conditions were fit over the range of 190–800nm and 190–880nm, respectively. The third condition corresponds to fits extending into the VUV (120–800nm). As is evident from these results, the differences between the first and second conditions are negligible. Hence, the extension of the conventional reflectance data set of the first condition by 80 nm at the long wavelength end (where the n and κ values are essentially flat) does nothing to improve measurement performance. The performance of condition 3 however, wherein the data set of condition 1 is extended by 70 nm into the VUV (where the n and κ values exhibit considerable structure) yields a very different result, reducing the 3σ uncertainty by a factor of 3.1 in n and 6.7 in κ. Conditions 4 – 6 present the results of fits performed on data files with a reflectance uncertainty of $1\sigma = 0.1\%$. Again the same trends are evident - extending the standard (190–800nm) reflectance data range by 80nm to longer wavelength does nothing to improve measurement performance, while extending by 70 nm into the VUV reduces the 3σ repeatability by a factor of 3.6 in n and 7.6 in κ.

Table 1 Summary of results obtained from fitting 100 simulated reflectance files based on 900Å photoresist with n and κ values at 193 nm equal to 1.71575 and 0.052138 respectively.

Photoresist Comparison						
Condition	1	2	3	4	5	6
Oscillators	1	1	1	1	1	1
Range (nm)	190-800	190-880	120-800	190-800	190-880	120-800
Added Noise (1σ)	0.20%	0.20%	0.20%	0.10%	0.10%	0.10%
Mean Thickness (Å)	899.96	899.95	899.95	900.00	900.00	900.00
Thickness 3σ	1.03802	0.99264	0.98018	0.48079	0.46992	0.43397
Mean n (193 nm)	1.71604	1.71600	1.71594	1.71596	1.71590	1.71578
n 3σ	0.00800	0.00799	0.00260	0.00443	0.00449	0.00119
Mean κ (193 nm)	0.05221	0.05218	0.05217	0.05221	0.05221	0.05215
κ 3σ	0.00290	0.00287	0.00043	0.00159	0.00162	0.00021

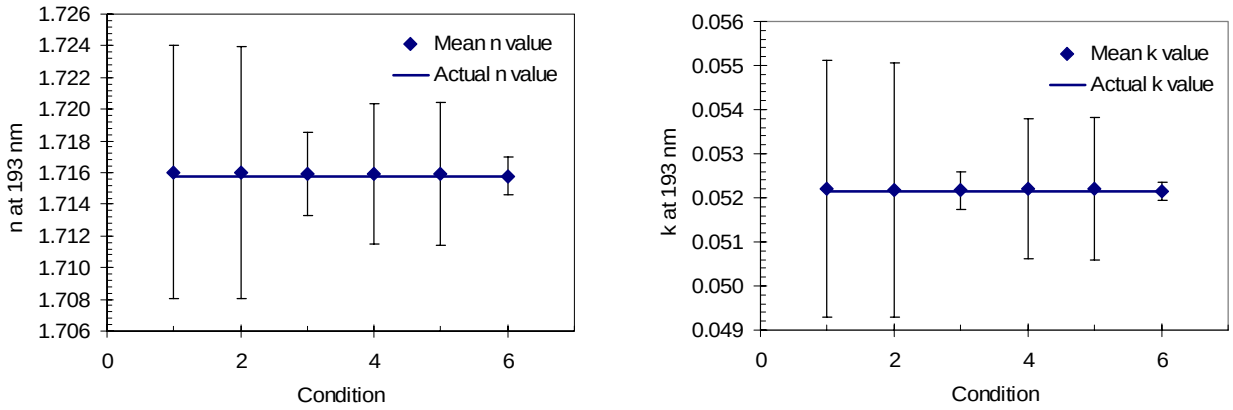

(a) (b)

Figure 7 Mean value of a) n, and b) κ at 193 nm obtained from fitting 100 simulated reflectance files based on a 900Å photoresist. Error bars represent +/- 3 sigma uncertainties.

The uncertainties in the index values are a direct consequence of the uncertainties in the Tauc-Lorentz parameters used to describe the film. Table 2 compares the 3-σ uncertainties for each of the 5 Tauc-Lorentz parameters for 190-800nm and 120-800nm data ranges for the 1 term resist example. The comparison shows that the uncertainties in Tauc-Lorentz parameters are reduced for the 120-800nm data by at least a factor of 4, and in many cases by an order of magnitude. The extent to which the Tauc-Lorentz uncertainties propagate into actual errors in measured n and κ values depends on the amount of constraint provided by the reflectance itself. For thicker films, changes in these parameters tend to affect the reflectance spectra everywhere in the 120-800 nm range, and the addition of VUV wavelength data serves to enhance sensitivity to changes in optical parameters and to reduce inter-parameter correlation, resulting in

more reliable n and κ measurements. As the film thickness decreases, the degree of uncertainty in n and κ increases as changes in film optical properties and thickness have less of an impact on 190-800 nm reflectance, to the point that determining both thickness and optical properties for a < 50-100 Å film *requires* 120-190 nm data, even if we're only trying to measure the optical properties for wavelengths greater than 190 nm.

Table 2 3-σ uncertainties for the 1 term resist Tauc-Lorentz parameters calculated from the 100x data for 190-800 nm reflectance and 120-800 nm reflectance. A random noise error of σ_i = 0.1% was assumed for the raw data in both cases.

	E_g (eV)	$\varepsilon_1(\infty)$	A (eV)	E_0 (eV)	C (eV)
190-800nm	0.031617	0.274983	14.731	1.4430	2.6138
120-800nm	0.0083061	0.027886	1.6428	0.10169	0.22171

The results from analysis of the 3-term BARC reflectance files are summarized in Table 3 and Figure 8. Conditions 1 and 2 in Table 3 correspond to fits performed on data files with a noise level of 1σ = 0.2% and fit over the range of 190–800 nm and 120–800 nm, respectively. As is evident, the extended VUV data set yields a significant reduction in measurement uncertainty of both n and κ. The data corresponding to conditions 3 – 5 represent the result of fits performed on data files with a noise level of 1σ = 0.1%. Once again the 120–800 nm data set outperforms the standard set of condition 3. The data corresponding to condition 4 results from fits performed using a 2-term Tauc-Lorentz dispersion rather than a 3-term dispersion to model the 190–800 nm data. The motivation for this condition follows from an examination of the n and κ spectra and simulated reflectance spectrum presented in Figures 9 and 10, which illustrate how structure in the VUV optical properties can play a subtle role in optical measurements performed at longer UV-Vis wavelengths.

Table 3 Summary of results obtained from fitting 100 simulated reflectance files based on 900 Å BARC film with n and κ values at 193 nm equal to 1.70304 and 0.212061 respectively.

BARC Comparison					
Condition	1	2	3	4	5
Oscillators	3	3	3	2	3
Wavelength Range (nm)	190-800	120-800	190-800	190-800	120-800
Added Noise (1σ)	0.20%	0.20%	0.10%	0.10%	0.10%
Mean Thickness (Å)	900.07	900.06	900.02	900.47	900.02
Thickness 3σ	0.86854	0.75791	0.46442	0.55658	0.39158
Mean n (193 nm)	1.70300	1.70294	1.70318	1.71281	1.70302
n 3σ	0.00603	0.00287	0.00380	0.00168	0.00131
Mean κ (193 nm)	0.21168	0.21189	0.21209	0.22878	0.21199
κ 3σ	0.00989	0.00358	0.00686	0.00302	0.00167

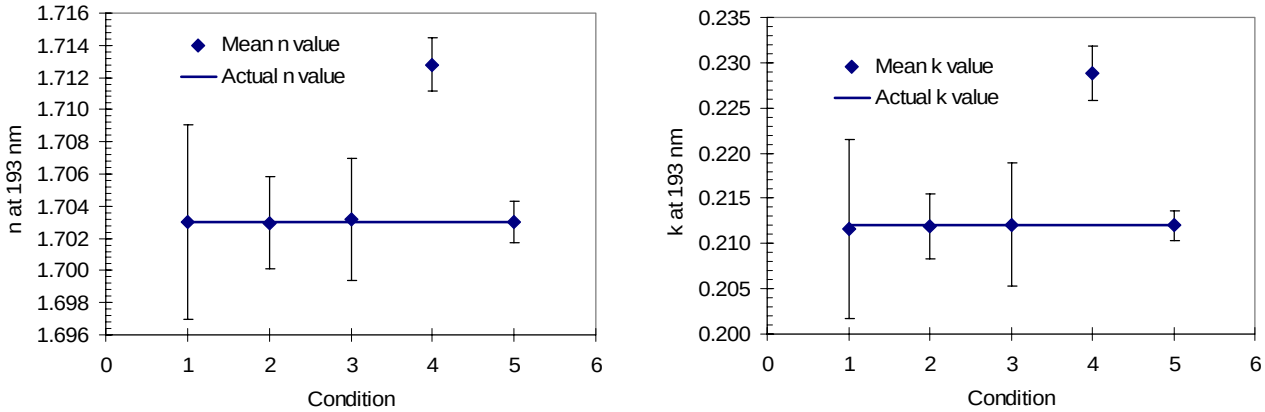

(a) (b)

Figure 8 Mean value of (a) n and (b) κ at 193 nm obtained from fitting 100 simulated reflectance files based on a 900 Å BARC. Error bars represent +/- 3 sigma uncertainties.

The solid lines in Figure 9 are the real and imaginary parts of the refractive index for the 3-term BARC material. The structure associated with an oscillator centered near 146 nm is apparent in the corresponding reflectance spectra, shown as the solid line in Figure 10. The corresponding curves for a 2-term BARC are shown as dashed curves in Figures 9 and 10. Above 190 nm, the reflectance from the 2 and 3-term models appear quite similar. Hence, without prior knowledge of the presence of the third oscillator in the VUV, conventional reflectometry users (only collecting data down to 190 nm) may lack incentive to include a third term in their description of the BARC. The results of this are shown in Table 3, condition 4. While the 2-term dispersion yields a better uncertainty statistic for the 190–800 nm case, the resulting systematic error causes the measured index to be completely erroneous.

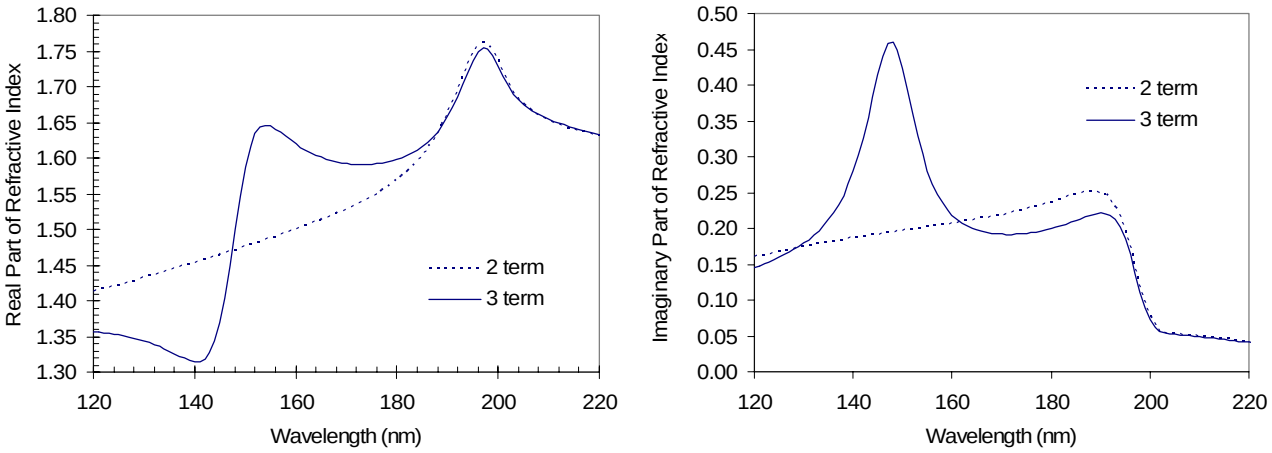

(a) (b)

Figure 9 Real (a) and imaginary (b) parts of the refractive index of BARC materials as described using 2-term and 3-term Tauc-Lorentz model.

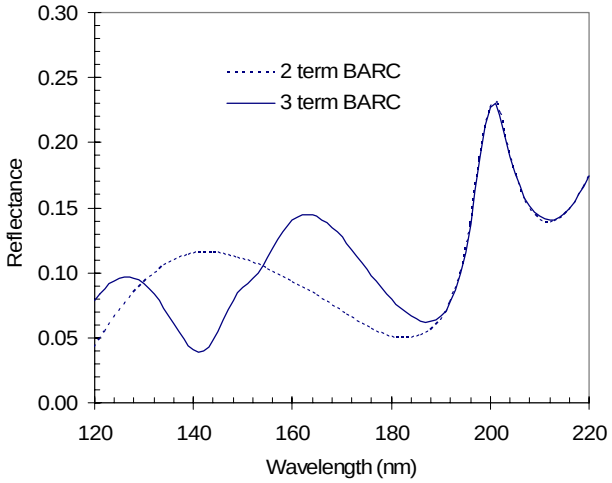

Figure 10 Simulated reflectance spectra for a 900Å BARC film based on 2-term and 3-term Tauc-Lorentz model.

4. Discussion/Conclusions

The results from the previous two sections can now be combined to examine the influence of metrology uncertainty on the effectiveness of a BARC at controlling reflectivity. The BARC studied above, which was based on an actual BARC material, is close to but not exactly an optimum second minimum BARC for 193nm resist on silicon. However, assuming that the fractional uncertainty in n and κ demonstrated in the simulated BARC of Section 3 is constant, the uncertainty in the optimum 90 nm second minimum BARC of Section 2 can be used. Table 4 shows the relevant refractive indices and uncertainties under this assumption.

Table 4 Conversion of n and κ uncertainty from the simulated BARC of Section 3 (0.2% noise case) to the optimum BARC of Section 2 under the assumption of constant relative uncertainty for both n and κ.

	Simulated BARC		Optimum BARC	
	190 – 800 nm range	120 – 800 nm range	190 – 800 nm range	120 – 800 nm range
n (193nm)	1.703	1.70294	1.691	1.691
σ_n	0.00201	0.00096	0.00200	0.00095
σ_n/n	0.00118	0.00056	0.00118	0.00056
κ (193nm)	0.21168	0.21189	0.3301	0.3301
σ_κ	0.00330	0.00119	0.00515	0.00186
σ_κ/κ	0.01559	0.00562	0.01559	0.00562

For the optimum 90 nm thick second-minimum BARC from Section 2, equation (10) becomes

$$R \approx 0.769\left|\Delta \boldsymbol{n}\right|^2 \tag{18}$$

For a 1-σ error in both real and imaginary parts of the refractive index, the resulting reflectivity (at 193nm) becomes

$$R \approx 0.769\left(\sigma_n{}^2 + \sigma_\kappa{}^2\right) \tag{18}$$

For a 3-σ error in both real and imaginary parts of the refractive index, the resulting reflectivity would be nine times larger. The results for reflectivity, for both the conventional 190 – 800 nm metrology and the VUV extended 120 – 800 nm metrology, are summarized in Table 5. The extended wavelength range results in a 7X reduction in the worst-case substrate reflectivity. For example, if a substrate reflectivity error of 0.01% is budgeted for BARC n and κ 3-σ metrology errors, then clearly the conventional 190 – 800 nm wavelength range with 0.2% added noise produces an unacceptably high reflectivity. Under the same conditions, however, the extended 120 – 800 nm wavelength range with its inherently higher noise tolerance produces reflectivities well within specifications. Note that no BARC thickness errors were included in this analysis, nor errors in photoresist optical properties. Since these errors will put the BARC film off of its minimum in reflectivity, the results presented here are a best case scenario.

Table 5 Resulting 1-σ and 3-σ worst-case reflectivities for the 0.2% added noise condition.

	190 – 800 nm range	120 – 800 nm range
σ_n	0.00200	0.00095
σ_κ	0.00515	0.00186
1-σ R (%)	0.00235	0.00034
3-σ R (%)	0.02115	0.00306

The analysis presented above shows how measurement noise propagates from the optical measurement of BARC n and κ to the resulting reflectivity of a BARC material. In particular, we have shown how the wavelength range used in optical measurements can impact the BARC optimization process. The analysis shows that extending the conventional UV-Vis metrology to VUV wavelengths can lead to a significant reduction of the substrate reflectivity error caused by metrology errors, showing that VUV metrology is a promising option for use in the characterization and selection of materials used in modern lithography. In addition, the distinct spectral features that are present in the vacuum ultraviolet region of the material optical properties could be used, for example, as a means of fingerprinting different lithography films that may otherwise appear to be identical if inspected at longer wavelengths. Finally, we point out that the improvements of VUV metrology over conventional metrology are expected to be even more pronounced for thinner films used in the fabrication of semiconductor devices.

Further studies in this area would include the impact of high angles of incidence on BARC performance, and the coupling of other error sources like photoresist and substrate optical properties.

5. References

1. C. A. Mack, Fundamental Principles of Optical Lithography: The Science of Microfabrication, John Wiley & Sons (*in press*).
2. W. H. Press, S. A. Teukolsky, W. T. Vetterling, and B. P. Flannery, Numerical Recipes in C: The Art of Scientific Computing, Second Edition, Cambridge University Press (Cambridge, MA: 1992).
3. G. E. Jellison and F. A. Modine, "Parameterization of the optical functions of amorphous materials in the interband region", *Appl. Phys. Lett.*, Vol. 69 (1996) p. 371.